On the Optimization of Cellular Networks for UAV Aerial Corridor Support

Matteo Bernabè, David Lopez-Perez, David Gesbert and Harvey Bao

***Abstract*—Cellular connected unmanned aerial vehicles (CCUAVs) are expected to enable new disruptive verticals with a significant impact on different business sectors. In particular, to enable connected and safe operations, the concept of drone corridors has recently received attention. In general, CCUAVs suffer from poor received signal strength, and they perceive large interference due to the high line-of-sight probability with the interfering sectors. In this paper, we propose an ADAM-based algorithm to optimize the electronic tilt of base stations deployed in an LTE network to improve the quality of service in predefined aerial corridors. Importantly, the numerical analysis results indicate that it is feasible to re-tune antenna sector directions to distribute, in an optimized manner, more power in the targeted corridors while minimizing interference, with a minimum impact for the ground, allowing usage of an already deployed LTE network for beyond line of sight (BLoS) communication.**

I. Introduction

Remotely pilot and equipped with sensors, unmanned aerial vehicles (UAVs) are set to change the world we are living in. Among others, they have already had a major impact on precision agriculture, surveillance and security as well as search and rescue [1], [2]. UAV technology will become commonplace in the following years, also disrupting our approaches to delivery and transportation. Packages, food and medicines will be delivered in a fast and safe manner with the use of UAVs. Autonomous flying taxis will redefine how we commute, and in turn, where we live and work. With these prospects, the value of the UAV industry has been estimated to reach USD 58.4 billion by 2026 [3]. More importantly, UAVs are expected to enable new disruptive verticals.

From a telecommunications perspective, UAV applications can be classified into 2 categories: *i)* UAV-aided networks, with UAVs as flying wireless network access points, and *ii)* cellular connected UAVs (CCUAVs), with UAVs connected to the network as flying user equipment (UE). Importantly, to support the growing CCUAV operations, governments and industries are looking at building the UAV highways of the sky. Thinking of them as sky lanes, this segregated aerospace can facilitate transformational opportunities within cities, as they provide a management —and importantly a legal— framework for the secure control and operation of UAVs [4], [5]. Supporting UAV highways with a reliable cellular connectivity will be a must to *i)* send/receive the required command and control (C&C) information to/from UAVs, and *ii)* pursue legislators to ease the current strict regulations on civilian pilot-less flights within cities, giving the green light to the new UAV markets [6]–[8].

978-1-6654-3540-6/22

Given a predefined fourth and/or fifth generation (4G/5G) cellular network, most CCUAV research has aimed at optimizing CCUAV aerial trajectories to support a given UAV quality of service (QoS), e.g., a 50 ms latency at 3 nines of reliability with 100 kbps capacity for C&C channels [9].

In [10], Bulut E. and Guevenc I. formulated an optimal CCUAV trajectory optimization problem under discontinuous signal reception constraints, and solved it, using dynamic programming. In [11], Challita U. *et al.* investigated an interference-aware CCUAV trajectory planning method, using an echo state network (ESN) as reinforcement learning (RL) framework to optimize time of flight, latency and caused interference. In [12], Esrafilian O. *et al.* proposed an optimal trajectory design for CCUAVs using a coverage map obtained by combining a 3D environment map and a radio propagation model. In [13], Bayerlein H. *et al.* put forward a framework for CCUAV trajectory optimization using an environment map, Internet of thing (IoT) data and RL to jointly minimise time of flight and collisions and maximize QoS over the path.

Despite the importance of UAV trajectory optimization, we envision, however, that aerial highways are more likely to be planned and deployed according to governmental and aerospace criteria, rather than purely connectivity ones [14]. Thus, optimizing third generation partnership project (3GPP) long term evolution (LTE) and new radio (NR) networks to support the required UAV QoS over a predefined UAV highway may be a more practical approach —and plausible business— than tailoring aerial corridors to existing networks. This different —and/or complementary— viewpoint requires for a different type of research than that presented earlier, and unfortunately, the literature is not extensive in this area of research, with only a limited number of pioneering works.

In [15], Maeng S. J. *et al.* provided a closed-form expression for the UAV signal-to-interference-plus-noise ratio (SINR)-based outage probability in a simple scenario with two ground BSs using uptilted antennas to optimize performance over defined air space regions. In [16], Chowdhury *et al.* proposed a ground network architecture with co-channel antennas oriented towards the sky and an enhanced inter-cell interference coordination (eICIC) technique to mitigate interference to/form the aerial corridors. In [17], Singh S. *et al.* investigated the optimal positioning of millimetre wave (mmWave) access points to provide connectivity on predefined aerial waypoints. In [18], Bhuyan A. *et al.* extended the previous work, additionally investigating the use of uplink non-orthogonal multiple access (NOMA) over predefined UAV trajectories to increase capacity and enhance physical layer security.

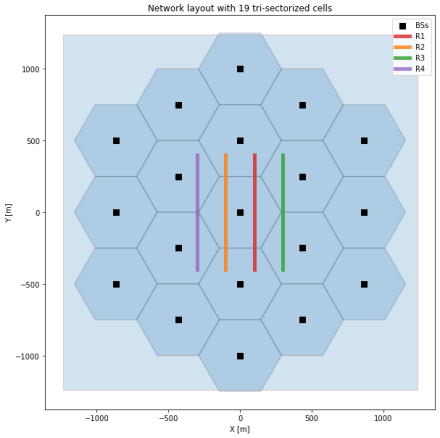

Fig. 1: Network Layout with 19 tri-sectorized cells with up to 4 aerial highways

Since NR deployments are still ramping up, and because LTE ones are the most widespread as of today, in this paper, we attempt to assess up to which extend a network operator can relay on LTE to support a reliable aerial highway connectivity, while having a minimum impact on its terrestrial performance. In more detail, we focus on the BS downtilt optimization problem, developing a light-weight large-scale stochastic network model suitable for optimization, and proposing an ADAM-based optimization framework to solve the stochastic optimization problem [19]. Using these tools, we analyse and quantify the benefits of segregated aerospace over traditionally assumed unconstrained CCUAV flights, as well as the gains of the proposed BS downtilt optimization.

The rest of the paper is organised as follows. In Section II, we define the system model. In Section III, we formulate our constrained maximization problem to tune the BS antenna downtilts and optimise aerial highway performance. In Section IV, we present the proposed algorithm. In Section V, we discuss the results. In Section VI, the conclusions are drawn.

II. System Model

This work considers a downlink LTE interference-limited scenario with terrestrial BSs and UEs as well as CCUAVs placed over predefined aerial routes. To drive our system-level analysis, we use the 3GPP macro urban models in [20], [21] for terrestrial UEs and those in [9] for CCUAVs.

A. Network Model

According to [20], 19 terrestrial BS sites at a height of 25 m are distributed in a 2-tier hexagonal grid with an inter-site distance (ISD) of 500 m, as shown in Figure 1. 3 sectors[1] per site are considered, thus having $N_{\mathrm{BS}} = 57$ sectors in our scenario. The operational carrier frequency is f_c, and we assume a bandwidth B_0, with a full frequency reuse in all cells. The transmission power per sector is P_0 [20].

To study the signal qualities in terms of SINR of both terrestrial UEs and CCUAVs, 2 regular square grids, k_g and k_a, are deployed at altitudes, h_g and h_a, respectively. For brevity, let us use k to denote any of these 2 grids in the sequel, i.e. $k = \{k_g, k_a\}$, and denote by N_k and d_k the number of grid points and the inter-grid point distance (IGD) in the k-th grid, respectively. Let us also denote by $k_u = k_g \cup k_a$ the set containing all the grid points of both grids, k_g and k_a, and by $N_u = N_g + N_a$ its cardinality.

With this notation, the vertical and horizontal antenna gain offsets between a sector $b \in \{1, \ldots, N_{\mathrm{BS}}\}$ and the location of a grid point $u \in \{1, \ldots, N_g\} \cup \{1, \ldots, N_a\}$, are presented in eqs. (1) and (2), respectively [20], i.e.

$$G^u_{b,\mathrm{Ver}}\left(\theta^u_b, \theta^{\mathrm{tilt}}_b\right) = -\min\left[12\left(\frac{\theta^u_b - \theta^{\mathrm{tilt}}_b}{\theta^{\mathrm{3dB}}}\right)^2, \mathrm{SLA_v}\right], \quad (1)$$

$$G^u_{b,\mathrm{Hor}}\left(\phi^u_b\right) = -\min\left[12\left(\frac{\phi^u_b - \phi^{\mathrm{bst}}_b}{\phi^{\mathrm{3dB}}}\right)^2, \mathrm{A_m}\right], \quad (2)$$

where θ^u_b is the relative angle in the zenith plane between the b-th sector and the u-th grid point, θ^{tilt}_b is the electrical antenna downtilt of the b-th sector, with values, for both angles, in $[-90°, +90°]$, θ^{3dB} is the vertical 3 dB beamwidth, $\mathrm{SLA_v}$ is the side-lobe attenuation in the vertical plane, ϕ^u_b is the relative angle in the azimuth plane between the b-th sector and the u-th point, with values in $[-180°, +180°]$, ϕ^{bst}_b is the boresight angle of the b-th sector, ϕ^{3dB} is the horizontal 3 dB beamwidth, and $\mathrm{A_m}$ is the side-lobe attenuation in the horizontal plane.

The total antenna gain offset can be then calculated as in eq. (3), i.e.

$$G\left(\theta^u_b, \theta^{\mathrm{tilt}}_b, \phi^u_b\right) = \quad (3)$$
$$-\min\left\{\left[G^u_{b,\mathrm{Ver}}\left(\theta^u_b, \theta^{\mathrm{tilt}}_b\right) + G^u_{b,\mathrm{Hor}}\left(\phi^u_b\right)\right], \mathrm{A_m}\right\}.$$

Note that in this paper, $\theta = 0°$ point towards the horizon, and G_0 is the maximum antenna gain.

Importantly, we use the grids, k_g and k_a, to drive the 2D spatially correlated lognormal stochastic process adopted to calculate the shadow fading realizations at each grid point u. In more details, we model shadowing through the sum of sinusoids (SOS) approach presented in [22] with the urban macro parameters specified in [21] for the ground grid k_g, and those in [9] for the aerial grid k_a. For completeness, note that σ^k_{SF} represents the standard deviation of the lognormal random variable governing the shadowing generation process in the k-th grid, and that, τ^u_b is used to refer to the stochastic shadow fading value of the b-th sector in the u-th grid point.

The line of sight (LoS) probability and the corresponding path loss ρ^u_b between the b-th sector and the u-th grid point are computed using the urban macro models specified in [21] for the ground grid k_g, and those in [9] for the aerial grid, k_a.

B. CCUAV Highways

In our analysis, we consider R aerial highways, and in contrast to [10]–[13], where the CCUAV trajectory is the result of an optimization process targeted at maximising UAV QoS, in our model, each aerial highway is simply represented by a straight line. This is because we assume that they have been a priori defined by an authority according to physical and

[1] In this paper, the terms sector and cell are used interchangeably.

not connectivity requirements, and thus requirements such as minimum time to target are the main design driver.

The aerial grid k_a is used to define the R aerial highways. A given aerial highway is represented as a collection of 'sequential' grid points on the aerial grid k_a. For convenience, let us denote by $k_r \in k_a$ the set of aerial grid points defining our R aerial highways, and by N_r its cardinality. Let us also denote by $k_e = k_g \cup k_r$ the set containing all grid points in grid k_g and set k_r, and by $N_e = N_g + N_r$ its cardinality. We will refer to k_e as the set of evaluation points in our network.

To avoid border effects, it is important to note that aerial highways have been deployed within —or around— the central site to capture the inter-cell interference from the 2 tiers of neighbouring cells. Moreover, to facilitate the analysis of results, the R aerial highways follow a symmetrical vertical deployment from Y_a to Y_b at different X_r positions. They are designed such that each route crosses multiple cell centers and edges to capture different network condition. All routes are depicted in Figure 1.

C. Received Signal Strength and Cell Association

To define the serving/interfering cells of the u-th grid point, a cell association rule based on the maximum received signal strength (RSS) is adopted. In more details, RSSs are calculated using eq. (4), while serving cells are found solving eq. (5), e.g.

$$\mathrm{RSS}_b^u = P_0 \rho_b^u \tau_b^u G_0 G_b^u \left(\theta_b^{\mathrm{tilt}}, \theta_b^u, \phi_b^u\right), \tag{4}$$

and

$$s^u = \underset{b}{\operatorname{argmax}} \left\{\mathrm{RSS}_b^u \mid b \in \{1, \ldots, N_{\mathrm{BS}}\}\right\}. \tag{5}$$

Once the best server is found, note that subscripts $\{s, i\}$ are used instead of subscript b to identify the serving and interfering cells, respectively. Using this notation, RSS_s^u is the received power from the serving cell $s \in \{1, ..., N_{BS}\}$ to the u-th point, while RSRP_i^u is that from the non-serving cell $i \in \{1, ..., N_{BS}\} \backslash s$ to the u-th point. Recall that, since the shadowing τ_b^u is a stochastic variable, both RSRP_b^u and s^u are stochastic variables too.

D. Signal to Interference Plus Noise Ratio

To assess the signal quality, the SINR γ^u evaluated at the u-th point is defined as follows:

$$\gamma^u\left(\boldsymbol{\theta}^{\mathrm{tilt}}, \boldsymbol{\theta}^u, \boldsymbol{\phi}^u, \boldsymbol{\tau}^u\right) = \frac{\rho_s^u \tau_s^u G_0 G_s^u \left(\theta_s^{\mathrm{tilt}}, \theta_s^u, \phi_s^u\right) P_0}{\sum_{i=1, i \neq s}^{N_{BS}} \rho_i^u \tau_i^u G_0 G_i^u \left(\theta_i^{\mathrm{tilt}}, \theta_i^u, \phi_i^u\right) P_0 + \sigma_n^2}, \tag{6}$$

where σ^2 is the noise power, and we use τ^u in the argument of γ^u to highlight the stochastic nature of the SINR. We consider that a grid point is out of coverage, if its SINR is below threshold $\gamma_{\mathrm{th}}^{\mathrm{out}}$.

Minimum CCUAV QoS requirements for CCUAV are reported in Table 5.1-1 of [9].

III. Tilt optimization of aerial highways

In this section, we propose an optimization framework to fine tune sector antenna downtilts with the objective of maximizing the overall average network performance, while guaranteeing a minimum QoS on the aerial highways.

The reason why we focus on the optimization of antenna downtilts is because strategically directing more power to the aerial highways through downtilt optimization helps alleviating one current major challenges to CCUAV QoS provisioning, i.e. the large interference perceived by them, resulting from the potentially large number of LoS interfering BSs —the higher the CCUAVs, the more the LoS interfering BS [8].

In more details, to find the best sector antenna downtilts for all N_{BS} sectors, we formulate a stochastic spectral efficiency maximization problem constrained to minimum aerial highway SINR requirements based on the system model described in Section II as follows:

$$\begin{aligned} \max_{\boldsymbol{\theta}^{\mathrm{tilt}}} \quad & \mathop{\mathbb{E}}_{\boldsymbol{\tau}^e}\left\{\sum_{e=1}^{N_e} \log\left(\log_2\left(1+\gamma^e\left(\boldsymbol{\theta}^{\mathrm{tilt}}, \boldsymbol{\theta}^e, \boldsymbol{\phi}^e, \boldsymbol{\tau}^e\right)\right)\right)\right\} \\ \text{s.t.} \quad & \mathop{\mathbb{E}}_{\boldsymbol{\tau}^r}\left\{\gamma^r\left(\boldsymbol{\theta}^{\mathrm{tilt}}, \boldsymbol{\theta}^r, \boldsymbol{\phi}^r, \boldsymbol{\tau}^r\right)\right\} \geq \gamma_{\mathrm{th}}^r, \\ & \forall r \in \{1, \ldots, N_r\}, \end{aligned} \tag{P1}$$

where the optimization parameters $\boldsymbol{\theta}^{\mathrm{tilt}}$ are the set of downtilt angles and, to prevent the algorithm from ending up in a solution where the points have extremely high or low performance, $\log(\cdot)$ is used for fairness.

Note that maximizing spectral efficiency over all grid points in set k_e aids at minimising the impact on terrestrial performance and providing the best performance to CCUAVs. Constraining on aerial highway SINR requirements, instead, allows for provisioning the required CCUAV QoS.

IV. Proposed Solution

Given the non-convex and stochastic nature of Problem (P1), and after analyzing multiple formulation and solvers (e.g. stochastic gradient descent (SGD), genetic programming), we reformulate the problem removing the constraint and using a utility $f^{(f)}(\cdot)$ and a penalty $g^{(f)}(\cdot)$ function to define the objective function $z^{(f)}$. We use an ADAM-based optimizer to solve the reformulated Problem (P2), where λ is the trade-off parameter between the mentioned utility and penalty functions, e.g. a higher λ gives more importance to fulfilling constraints.

$$\begin{aligned} \max_{\boldsymbol{\theta}^{\mathrm{tilt}}} z\left(\boldsymbol{\theta}^{\mathrm{tilt}}\right) = \sum_{f}^{N_{\mathrm{SF}}} f^{(f)}\left(\boldsymbol{\theta}^{\mathrm{tilt}}, \boldsymbol{\tau}^{e,(f)}\right) - g^{(f)}\left(\boldsymbol{\theta}^{\mathrm{tilt}}, \boldsymbol{\tau}^{r,(f)}\right) = \\ \sum_{f}^{N_{\mathrm{SF}}}\left(\sum_{e=1}^{N_e} \log\left(\log_2\left(1+\gamma^{e,(f)}\left(\boldsymbol{\theta}^{\mathrm{tilt}}, \boldsymbol{\theta}^e, \boldsymbol{\phi}^e, \boldsymbol{\tau}^{e,(f)}\right)\right)\right) - \right. \\ \left. \lambda \cdot \sum_{r}^{N_r} \mathrm{ReLU}\left[\gamma_{\mathrm{th}}^r - \gamma^{r,(f)}\left(\boldsymbol{\theta}^{\mathrm{tilt}}, \boldsymbol{\theta}^r, \boldsymbol{\phi}^r, \boldsymbol{\tau}^{r,(f)}\right)\right]\right). \end{aligned} \tag{P2}$$

It should be noted that the selected ADAM-based optimizer is a well-know method to efficiently solve non-convex stochastic

problems with a sparse gradient. In more detail, ADAM is an extension of SGD, which computes individual adaptive learning rates for different parameters from estimates of first and second moments of the gradient [19].

In Algorithm 1, we present the details of the implementation of our ADAM-based algorithm.

Algorithm 1: ADAM Based Algo for Antenna Tilts

```
Init network layout, grids points and aerial highways;
Init tilt angles θ^tilt ← θ^tilt_3GPP;
Init opt hyper-parameters;
Compute cell association;
Sectors selection;
l ← 0;
for i in N_Iter do
    Obj func z ← 0;
    for f in N_SF do
        Compute channel realization ρ^u_b, τ^{u,(f)}_b;
        Compute SINR γ^{e,(f)}_opt;
        Compute intermediate Obj func z^(f) of the f-th realization;
        z ← z + z^(f);
    end
    Compute ADAM gradient from Obj func z;
    Update selected sector antenna downtilts θ^tilt ← θ^tilt_ADAM;
    if |∇z^(j)| ≤ ε, ∀j ∈ {i, ..., i − t} and l > L_max then
        l ← 0;
        Compute cell association;
    else if |∇z^(j)| ≤ ε, ∀j ∈ {i, ..., i − t} and l ≤ L_max then
        Save intermediate solution;
        Explore solution space θ^tilt ← θ^tilt_3GPP + U(−20°, 0°);
        p ← p + 1;
        if p = P_max then
            break;
        end
    l ← l + 1;
end
From the intermediate saved solution select the final one;
```

First, the proposed algorithm builds over the system model presented in Section II, realising all important variables. Importantly, sector antenna downtilts are initialized with the values suggested in [20], i.e. $\boldsymbol{\theta}^{\text{tilt}}_{\text{3GPP}}$. Once the play ground is set, the optimization hyper-parameters are initialized, and the serving sector is found for every evaluation point. Then, before any gradient computation occurs, we implement a sector selection process to decompose the complexity of the optimization problem. In more detail, this process, based on aerial route knowledge and geometry calculations, is used to reduce the set of sector antenna downtilts to adjust in the optimization. Using this process, not only the speed of the algorithm is improved, but it also allows it to operate over a more 'local' objective function with a smoother shape, which in turn, enhances the performance of our ADAM optimizer. Once the sectors to optimise are selected, an optimization loop comprised at most of N_{Iter} iterations is performed. At each iteration, first, the cumulative objective function z is set to zero, and then, to embrace the stochastic nature of our problem, the algorithm iterates over N_{SF} spatially correlated shadow fading realizations, using the inner loop. For each such iteration, the SINR $\gamma^e \in k_e$, together with the objective function $z^{(f)}$ of the particular f-th shadow fading realization, are calculated and accumulated in the cumulative objective function z. Then, the ADAM gradient is calculated from z, and the selected sector antenna downtilts are updated consequently.

Importantly, it should be noted that updating sector antenna downtilts may change best serving cell. Thus, to aid the optimizer to escape from spurious local maximum, caused by this suboptimal cell association, the algorithm subsequently checks if z has reached a quasi-stationary condition, and, if so, a new cell association process is performed. The parameter ϵ is used to control the quasi-stationary condition and this cell re-association process. In particular, two conditions are checked, whether the value of the norms of the objective gradient $|\nabla z|$ has remained below the threshold ϵ for t iterations, and if the number of iterations l from the previous cell re-association is greater than $L_{\max}$. If these two conditions are true, the iteration counter l is set to zero, and an association process is carried out. If only the first condition is true, we assume that the optimization has converged, and the algorithm saves the intermediate solution. Moreover, to continue exploring the solution space, it jumps to another sector antenna downtilts initial configuration. The new initial value will be the one suggested in [9] plus a random component uniformly distributed. After $P_{\max}$ explorations the iteration terminates.

Finally, among the intermediate solutions saved, the final one is selected such that most of the constraints are satisfied, and the objective function is maximised.

V. Evaluation and Discussion

In the following, we present the results obtained when using the algorithm introduced in Section IV on the system model defined in Section II. In particular, we investigate:

A) how different aerial highway altitudes impact system performance, in terms of 5% percentile and average SINR gains. In more details, we compare optimized results with those obtained using the sector antenna downtilts suggested by the 3GPP in [20], i.e. $\boldsymbol{\theta}^{\text{tilt}} = \boldsymbol{\theta}^{\text{tilt}}_{\text{3GPP}}$. We also provide an analysis on the impact of our optimization to terrestrial grid points SINRs.

B) The benefits of using aerial highways with respect to unconstrained CCUAV flights, equivalent to a random CCUAV deployment, in terms of SINR gains and the number of PRBs needed to fulfil the minimum CCUAV QoS requirements.

C) The CCUAV performance when an increasing number of aerial highways are deployed in the network.

As baseline minimum CCUAV QoS requirement, we set minimum throughput $\text{T}_{\text{C\&C}} = 100\,\text{kbps}$ [9]. Using $\text{N}_{\text{PRB}} = 1$ physical resource block (PRB) with $B_{\text{PRB}} = 180\,\text{KHz}$, and using the Shannon theorem together with a safety margin of $80\,\text{kbps}$, we obtain $\gamma^r_{\text{th}} = 0\,\text{dB}$ as a minimum required SINR for each aerial evaluation point.

Table I presents the parameters and the values used in this experimental evaluation.

A. Impact of different altitude on the SINR performance

Figure 2 shows the SINR distributions of the aerial evaluation points placed in R1 (see Figure 1) for different altitudes

Param	Value	Param	Value
ISD	500 m	X_r	$\{\pm 100, \pm 200\}$ m
N_{BS}	57	$\sigma_{\text{SF}}^{\text{kg,(LoS)}}$	4 dB
f_c, B_0	2.6 GHz, 20 MHz	$\sigma_{\text{SF}}^{\text{kg,(NLoS)}}$	6 dB
P_0, G_0	43 dBm, 14 dBi	$\sigma_{\text{SF}}^{\text{ka,(LoS)}}$	{3.34,2.40,1.72,1.24} dB
h_g	1.5 m	$\sigma_{\text{SF}}^{\text{ka,(NLoS)}}$	6 dB
h_a	{50,100,150,200} m	R	{1,2,3,4}
IGD	25 m	N_r	{33,66,99,132}
N_g, N_a	6780, 6780	$\gamma_{\text{th}}^{\text{out}}$, γ_{th}^{r}	-6, 0 dB
$\theta_{\text{3GPP}}^{\text{tilt}}$	15°	λ	$2 \cdot 10^6$ bits/sec/Hz
θ^{3dB}	10°	ADAM Lr	0.1
ϕ^{3dB}	70°	N_{Iter}, N_{SF}	1000, 100
ϕ^{bst}	{30°, 150°, 270°}	ϵ, t	10^{-3}, 10
SLA_{v}	20 dB	$L_{\max}$, $P_{\max}$	20, 2
A_m	25 dB	B_{PRB}	180 KHz
Y_a, Y_b	-400 m, +400 m	$\text{T}_{\text{C\&C}}$	100 Kbps

TABLE I: Parameters values summary

h_a and for both the optimized and none optimized cases. From this figure, it can be seen that the mean value of

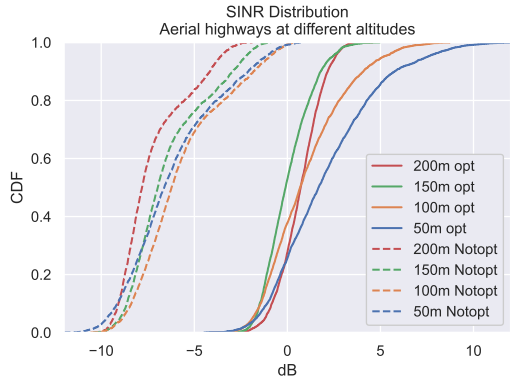

Fig. 2: Aerial points SINR distribution at different altitude with $R = 1, N_r = 33, \gamma_{\text{th}}^{r} = 0\,\text{dB}$

the SINR of the CCUAVs for the none optimized case decreases as the altitude increases, going from $-6.14\,\text{dB}@50\,\text{m}$ to $-7.25\,\text{dB}@200\,\text{m}$. This is due to the increasing inter-cell interference, as the higher the aerial highway the larger the LoS probability. This is in line with the results in [8].

With regard to our optimization, the results show that it introduces significant average gains of 7.61 dB and 7.33 dB at the 5% percentile and mean SINR, respectively. This is due to the enhanced signal power and mitigated inter-cell interference towards the aerial highway. For completeness, Table II provides a summary of such gains.

Aerial 5% Perc SINR	**50m**	**100m**	**150m**	**200m**
Opt [dB]	-1.65	-1.87	-1.73	-1.19
Not Opt [dB]	-9.70	-8.85	-8.99	-9.34
Gain [dB]	8.05	6.98	7.26	8.15
Aerial Mean SINR	**50m**	**100m**	**150m**	**200m**
Opt [dB]	2.07	1.01	0.05	0.69
Not Opt [dB]	-6.14	-5.69	-6.41	-7.25
Gain [dB]	8.21	6.71	6.46	7.94
Ground 5% Perc SINR	**50m**	**100m**	**150m**	**200m**
Opt [dB]	-1.54	-1.62	-1.58	-1.67
Not Opt [dB]	-1.21	-1.21	-1.21	-1.21
Gain [dB]	-0.34	-0.41	-0.36	-0.46

TABLE II: Summary of the aerial and ground points SINR performances for different altitudes

Considering the optimized curves, despite the clear decreasing trend with the aerial highway height at the head of the distribution, the 5% percentiles values are similar. This result is driven by the evaluation points placed at the cell edge, whose performance is hard to optimize regardless of the altitude.

To analyze the impact of our optimization on the ground network, Table II reports the 5% percentile SINR of the terrestrial evaluation points, while considering different aerial highway altitudes. As expected, optimizing the ground network for aerial usage negatively impacts the ground performance, and such impact is larger at the cell edge. However, the impact is not major, with an average performance loss of $-0.39\,\text{dB}$ (detailed values are reported in Table II).

B. Aerial Highways Benefits

To show the benefits of segregating aerial space for CCUAVs, we compare two optimization frameworks. In the first framework, we uniformly drop N_r aerial evaluation points, and optimize the ground network for them. Once the network is optimized, to simulate random movement of CCUAVs, we perform 100 new drops of N_r aerial evaluation points in new random positions, and we evaluate network CCUAV performance for each new drop. We do not optimize the network at each new random position, because, in reality, antenna downtilts can not be optimized dynamically. In the second framework, we consider our aerial highways, with N_r aerial evaluation points placed over R1 (see Figure 1) at an altitude of 150 m. The obtained SINR distributions are shown in Figure 3. Analyzing the results, we can state that optimizing

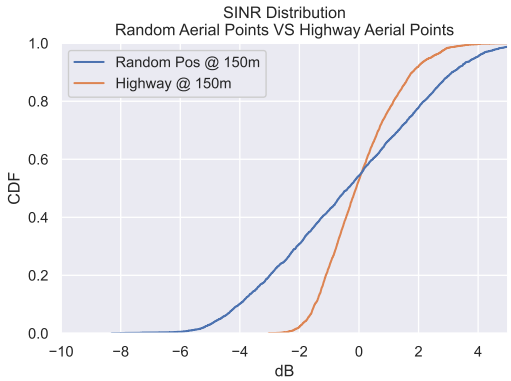

Fig. 3: Comparison of SINR distribution of random aerial point positions and aerial highway points with $R = 1, N_r = 33, \gamma_{\text{th}}^{r} = 0\,\text{dB}$

aerial highways allow for a more secure CCUAV performance, with a gain of 2.93 dB at the 5% percentile SINR. To put this gain in perspective, it should be noted that, to achieve the set requirement of $\text{T}_{\text{C\&C}} = 100\,\text{kbps}$ with such 5% percentile SINRs, 2 PRBs per CCUAV are needed for the unconstrained CCUAV framework, while only 1 is required when using aerial highways. This means that the aerial highway framework can support double the CCUAVs.

C. Impact of multiple highways

In the following, we analyse how the performance evolves when deploying multiple aerial highways in the same area. We

consider two scenarios: 2 routes symmetrically deployed in the network center (inner routes in Figure 1), and all 4 routes. The obtained SINR distributions are shown in Figure 4.

Although increasing the number of aerial highways linearly increases the number of flying CCUAVs, it also leads to a worse performance in each one of them. In particular, for the 2 routes scenario, we obtain, at the 5% percentile and mean SINR, -1.60 dB and 0.83 dB, respectively. Instead, for the 4 routes scenario, we respectively get -1.83 dB and 0.20 dB. A maximum loss of 0.92 dB is achieved at the 56% percentile.

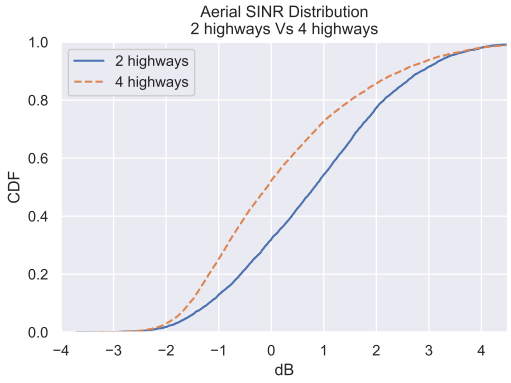

Fig. 4: SINR Performances for 2 and 4 highways at 150 m

This performance loss is due to the limited degrees of freedom of the network to satisfy the more aerial evaluation points — a more complex problem. In more details, it is harder to simultaneously bring more power to a larger number of aerial evaluation points. Moreover, the more signal power brought in a highway increases now the interference towards the aerial points of neighboring highways.

These results show how authorities and network operators should carefully decide the number of aerial highways to deploy in an area, as more highways bring more capacity and choice, but may, at some point, compromise performance.

VI. Conclusion

In this paper, we have proposed an ADAM-based algorithm to fine tune the antenna downtilts of an LTE terrestrial network to optimize QoS on predefined aerial highways. Our results indicated that it is feasible to re-tune antenna sector directions to distribute, in an optimized manner, more power in the sky while minimizing interference, with a minimum impact in the ground network. This allows for the usage, to some extend, of an already deployed LTE network for reliable BLoS communication. However, from all numerical results presented in this paper, it should also be noted that, it was not possible to always satisfy minimum SINR constraints. This is mainly due to the existence of challenging cell edge aerial evaluation points, and because our LTE network, through the analysed downtilt optimization, does not have the flexibility to simultaneously direct power and mitigate inter-cell interference towards a large number of directions. Future work will integrate different 5G beamforming and interference mitigation techniques to further enhance overall aerial performance.

References

[1] D. Floreano and R. J. Wood, "Science, technology and the future of small autonomous drones," *Nature*, vol. 521, pp. 460–466, 2015.

[2] Y. Zeng, J. Lyu, and R. Zhang, "Cellular-Connected UAV: Potential, Challenges, and Promising Technologies," *IEEE Wireless Commun.*, vol. 26, no. 1, pp. 120–127, 2019.

[3] MarketsandMarkets, "Unmanned Aerial Vehicle (UAV) Market by Point of Sale, Systems, Platform (Civil Commercial, and Defense Governement), Function, End Use, Application, Type, Mode of Operation, MTOW, Range, and Region - Global Forecast to 2026," Jun. 2021.

[4] Amazon. (2015) Revising the Airspace Model for the Safe Integration of Small Unmanned Aircraft Systems.

[5] N. Cherif, W. Jaafar, H. Yanikomeroglu, and A. Yongacoglu, "3D Aerial Highway: The Key Enabler of the Retail Industry Transformation," *IEEE Commun. Mag.*, vol. 59, no. 9, pp. 65–71, 2021.

[6] A. Fotouhi, H. Qiang, M. Ding, M. Hassan, L. G. Giordano, A. Garcia-Rodriguez, and J. Yuan, "Survey on UAV Cellular Communications: Practical Aspects, Standardization Advancements, Regulation, and Security Challenges," *IEEE Commun. Surveys Tutorials*, vol. 21, no. 4, pp. 3417–3442, 2019.

[7] G. Geraci, A. Garcia-Rodriguez, M. M. Azari, A. Lozano, M. Mezzavilla, S. Chatzinotas, Y. Chen, S. Rangan, and M. Di Renzo, "What Will the Future of UAV Cellular Communications Be? A Flight from 5G to 6G," 2021.

[8] A. Garcia-Rodriguez, G. Geraci, D. Lopez-Perez, L. G. Giordano, M. Ding, and E. Bjornson, "The Essential Guide to Realizing 5G-Connected UAVs with Massive MIMO," *IEEE Commun. Mag.*, vol. 57, no. 12, pp. 84–90, 2019.

[9] 3GPP TR 36.777, "Enhanced LTE support for aerial vehicles," Jan. 2017, v. 15.0.0.

[10] E. Bulut and I. Guevenc, "Trajectory Optimization for Cellular-Connected UAVs with Disconnectivity Constraint," in *IEEE International Conference on Communications Workshops (ICC Workshops)*, 2018.

[11] U. Challita, W. Saad, and C. Bettstetter, "Deep Reinforcement Learning for Interference-Aware Path Planning of Cellular-Connected UAVs," in *IEEE International Conference on Communications (ICC)*, 2018.

[12] O. Esrafilian, R. Gangula, and D. Gesbert, "3D-map assisted UAV trajectory design under cellular connectivity constraints," in *IEEE International Conference on Communications (ICC)*.

[13] H. Bayerlein, M. Theile, M. Caccamo, and D. Gesbert, "Multi-UAV Path Planning for Wireless Data Harvesting With Deep Reinforcement Learning," *IEEE Open Journal of the Communications Society*, vol. 2, pp. 1171–1187, 2021.

[14] F.A.A., *Pilot's Handbook of Aeronautical knowledge*, 2016.

[15] S. J. Maeng, M. M. U. Chowdhury, Güvenç, A. Bhuyan, and H. Dai, "Base Station Antenna Uptilt Optimization for Cellular-Connected Drone Corridors," 2021.

[16] M. M. U. Chowdhury, I. Guvenc, W. Saad, and A. Bhuyan, "Ensuring Reliable Connectivity to Cellular-Connected UAVs with Up-tilted Antennas and Interference Coordination," 2021.

[17] Singh, Simran and Bhattacherjee, Udita and Ozturk, Ender and Güvenç, İsmail and Dai, Huaiyu and Sichitiu, Mihail and Bhuyan, Arupjyoti, "Placement of mmWave Base Stations for Serving Urban Drone Corridors," in *IEEE Vehicular Technology Conference (VTC)*, 2021.

[18] A. Bhuyan, Güvenç, H. Dai, M. L. Sichitiu, S. Singh, A. Rahmati, and S. J. Maeng, "Secure 5G Network for a Nationwide Drone Corridor," in *IEEE Aerospace Conference*, 2021.

[19] D. P. Kingma and J. Ba, "Adam: A Method for Stochastic Optimization," 2014.

[20] 3GPP TR 36.814, "Evolved Universal Terrestrial Radio Access (E-UTRA); Further advancements for E-UTRA physical layer aspects," Mar. 2017, v. 9.2.0.

[21] 3GPP TR 38.901, "Study on channel model for frequencies from 0.5 to 100 GHz," Mar. 2017, v. 14.0.0.

[22] X. Cai and G. Giannakis, "A two-dimensional channel simulation model for shadowing processes," *IEEE Trans. on Vehicular Tech.*, vol. 52, no. 6, pp. 1558–1567, 2003.